
Modeling Gene Expression Distributional Shifts for Unseen Genetic Perturbations

Kalyan Ramakrishnan
University of Oxford

Jonathan G. Hedley¹
University of Oxford

Sisi Qu
University of Oxford

Puneet K. Dokania
University of Oxford

Philip H. S. Torr
University of Oxford

Cesar A. Prada-Medina
Novo Nordisk

Julien Fauqueur
Novo Nordisk

Kaspar Märtens²
Novo Nordisk

Abstract

We train a neural network to predict distributional responses in gene expression following genetic perturbations. This is an essential task in early-stage drug discovery, where such responses can offer insights into gene function and inform target identification. Existing methods only predict changes in the mean expression, overlooking stochasticity inherent in single-cell data. In contrast, we offer a more realistic view of cellular responses by modeling expression distributions. Our model predicts gene-level histograms conditioned on perturbations and outperforms baselines in capturing higher-order statistics, such as variance, skewness, and kurtosis, at a fraction of the training cost. To generalize to unseen perturbations, we incorporate prior knowledge via gene embeddings from large language models (LLMs). While modeling a richer output space, the method remains competitive in predicting mean expression changes. This work offers a practical step towards more expressive and biologically informative models of perturbation effects.

1 Introduction

Predicting changes in gene expression in response to genetic perturbations is a central goal in functional genomics and early-stage drug discovery. The aim is to understand how perturbing a gene (by switching it off, reducing its activity, or increasing its expression) affects the expression of other genes across the genome. Gene expression is stochastic – even in genetically identical cells, levels fluctuate due to transcriptional noise, regulatory variation, and measurement uncertainty (Paulsson, 2005; Raj and van Oudenaarden, 2008). Thus, gene expression is best modeled as a distribution across cells, a crucial aspect many methods overlook.

Evidence for the complexity of gene expression distributions comes from both observational and interventional data. For example, de Torrenté et al. (2020) analyzed gene expression profiles from the Cancer Genome Atlas³ and cataloged a wide range of distribution shapes that more accurately reflect biological variation. Incorporating these patterns into predictive models improved downstream tasks such as cancer survival prediction. Similar distributional diversity is seen in controlled perturbation experiments. Recent techniques such as Perturb-seq (Dixit et al., 2016; Norman et al., 2019; Replogle et al., 2022) enable expression profiling across thousands of single cells following genetic

¹jonathan.hedley@eng.ox.ac.uk

²KQTM@novonordisk.com

³<https://www.cancer.gov/tcga>

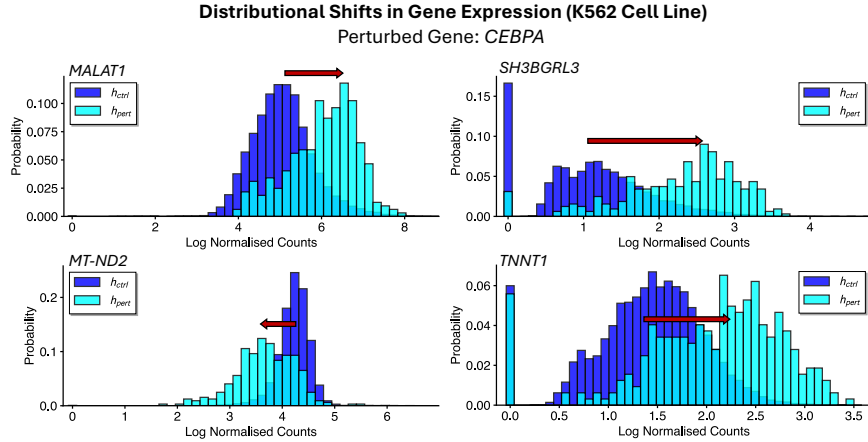


Figure 1: Gene expression distributional shifts following a *CEBPA* perturbation in the K562 cell line for four example genes. In each case, the control (dark blue) and perturbed (cyan) histograms differ in the mean *and* overall shape, including variance, skewness, zero inflation, and multimodality.

perturbations (gene knockouts), revealing shifts in mean expression, as well as in variance, skewness, and modality (Fig. 1). However, experimentally profiling every possible perturbation in all cellular contexts is prohibitively expensive and time-consuming. This motivates the development of *in silico* models that can predict responses to unseen perturbations, enabling generalization beyond the limited set of experimentally measured conditions.

Several deep generative models have been developed to predict gene expression responses to perturbations. CPA (Lotfollahi et al., 2023) and sVAE+ (Lopez et al., 2023) use latent-variable architectures with probabilistic decoders but rely on fixed parameterized likelihoods that may be too rigid to capture the diversity of expression patterns in real data (de Torrenté et al., 2020). More critically, they lack mechanisms for generalizing to unseen perturbations, limiting their use in exploratory perturbation response prediction (Wu et al., 2024).

Other works focus on generalization by incorporating prior biological knowledge. GEARS (Roohani et al., 2024) uses gene ontology and co-expression graphs to propagate perturbation signals to related genes. Foundation models, such as scGPT (Cui et al., 2024) and scFoundation (Hao et al., 2024), rely on transformers trained on large observational single-cell atlases to learn gene and cell embeddings. Despite their scale, these models only predict shifts in the mean and ignore distributional changes. Moreover, Ahlmann-Eltze et al. (2024) show that these sophisticated models fail to outperform simple linear baselines when evaluated on out-of-distribution (OOD) perturbations. This suggests that scale and architectural complexity alone are insufficient for generalizable response prediction, motivating a shift toward simpler yet biologically grounded alternatives.

A promising direction is to embed prior knowledge directly into model inputs, enabling generalization via functional similarity. Large language model (LLM)-informed gene embeddings, derived from protein sequences, ontologies, or expression corpora, can capture functional relationships between genes (Rives et al., 2021; Theodoris et al., 2023). By conditioning perturbation models on these embeddings, responses may be inferred for genes not seen during training. Märtens et al. (2024) demonstrate that utilizing LLM-based embeddings significantly enhances OOD performance; however, their model only predicts mean expression changes.

We address the above limitations by (i) predicting gene expression distributions and (ii) generalizing to unseen perturbations. To our knowledge, no existing method jointly tackles both. Our simple framework combines LLM-informed gene embeddings with a flexible histogram-based output, approximating per-gene expression distributions using discretized bins. On single-cell datasets (Norman et al., 2019; Replogle et al., 2022), this simple model outperforms other distributional baselines with as few as 15 bins and trains $\sim 3x$ faster. The richer output enables more informative analyses than mean shifts, such as identifying distinct responses to the same perturbation or estimating prediction uncertainty, helping better understand how genes influence one another.

2 Related Work

Generative models for perturbation effects. Generative models are widely used to simulate transcriptional responses in single cells. scVI (Lopez et al., 2018) models gene expression counts with a negative binomial VAE (Kingma et al., 2013) to capture measurement noise and variability across cells. scGen (Lotfollahi et al., 2019) and CPA (Lotfollahi et al., 2023) learn latent-space shifts that encode perturbation effects, enabling interpolation across conditions. sVAE+ (Lopez et al., 2023) and SAMS-VAE (Bereket and Karaletsos, 2023) separate baseline and perturbation components to improve interpretability, while CellOT (Bunne et al., 2023) aligns control and perturbed populations via neural optimal transport. However, all remain limited to perturbations seen during training.

Generalization to unseen perturbations. Generalizing to unseen perturbations is critical for scalable profiling. GEARS (Roohani et al., 2024) addresses this by propagating perturbation signals over a gene ontology graph. More recently, foundation models such as scGPT (Cui et al., 2024) and scFoundation (Hao et al., 2024) learn gene and cell embeddings from large-scale data using transformers. Despite their scale, these models predict only mean responses and do not model distributions. Moreover, a recent benchmark (Ahlmann-Eltze et al., 2024) shows they struggle to outperform simple baselines on OOD perturbations.

Gene embeddings from language models. Pretrained language models have recently been adopted to encode biological priors. GenePT (Chen and Zou, 2024) generates embeddings from NCBI gene descriptions⁴ and shows that these embeddings encode underlying biology, e.g., gene function. Märtens et al. (2024) incorporate similar embeddings into perturbation models, demonstrating state-of-the-art generalization to unseen targets. However, all focus exclusively on mean responses.

3 Method

3.1 Overview

We aim to model responses to genetic perturbations by learning a conditional distribution over gene expression values given a perturbation $p \in \{0, 1\}^P$, where P is the number of perturbable genes. Let $\mathbf{x} \in \mathbb{R}_{\geq 0}^G$ be a random vector representing post-perturbation log-normalized expression across G genes. The task is to approximate the conditional distribution $q(\mathbf{x}|p)$. In principle, this is a joint distribution over all genes, residing in a high-dimensional space that is challenging to model directly (partly due to the sparsity and noise inherent in single-cell data). We therefore focus on predicting gene-wise marginal distributions $q(x_g|p)$ for each gene g . While this ignores gene-gene correlations, it allows tractable distribution modeling and captures per-gene variability across cells.

3.2 Histogram Construction

To represent marginal expression distributions, we discretize each gene’s expression range into a constant number of fixed-width bins and model the result as a histogram. Thus, we approximate $q(x_g|p) \approx h(x_g|p)$, where h is a piecewise uniform density over the expression range.

For each gene g , expression values in the training data (across all perturbations) are binned into B intervals of width w_g . The test data is discretized using the same bin edges to prevent data leakage. Expression ranges are symmetrically extended by a small constant ϵ_g to avoid truncation:

$$r_g = [\min(x_g) - \epsilon_g, \max(x_g) + \epsilon_g], \quad \text{where} \quad \epsilon_g = \frac{\max(x_g) - \min(x_g)}{2(B - 1)} \quad (1)$$

and the minimum and maximum values are calculated per gene from the training data. This choice of ϵ_g ensures the first bin is centered at the minimum, allowing the model to assign mass exactly at zero to better capture the sparsity in single-cell data. For genes with a constant expression (e.g., all zeros), we assign a small positive upper bound to avoid degenerate binning and ensure non-negative support. Histograms are then computed by assigning a probability mass to each bin based on the fraction of cells falling within it, yielding a valid discrete distribution.

⁴<https://www.ncbi.nlm.nih.gov/gene>

3.3 LLM-informed Perturbation Encoding

We map each perturbation p to a continuous vector $\mathbf{e}_p \in \mathbb{R}^d$ using a fixed function, where d is the embedding dimension. For this, we first extract embeddings for each perturbed gene from the following two sources, building on the success of LLM-based models from Märtens et al. (2024):

- (i) **Gene descriptions:** Text embeddings of NCBI gene descriptions from GPT-3.5, as proposed by Chen and Zou (2024).
- (ii) **Protein sequences:** Sequence embeddings from the ProtT5 (Elnaggar et al., 2022) protein language model.

We concatenate both types following Märtens et al. (2024). These gene embeddings are frozen while training and serve as biologically informed inputs to enable generalization to unseen perturbations. If several genes are perturbed simultaneously, we could aggregate their embeddings via a simple average. However, we restrict ourselves to single-gene perturbations in this work.

3.4 Model Architecture

Given a perturbation, we model the induced *distributional shift* in gene expression relative to an empirically observed control (unperturbed) distribution. This reflects the biological intuition that most perturbations modify, rather than overwrite, a cell’s baseline expression profile. Let $h_{\text{ctrl}} \in \mathbb{R}^{G \times B}$ denote the control histogram, where each row (summing to 1) contains the baseline distribution of a gene over the B bins. For a perturbation p , we apply shifts $\Delta \in \mathbb{R}^{G \times B}$ in log space as follows:

$$\hat{h}_\theta(p) = \text{softmax}(\log h_{\text{ctrl}} + \Delta_\theta(\mathbf{e}_p)), \quad (2)$$

where $\Delta_\theta : \mathbb{R}^d \rightarrow \mathbb{R}^{G \times B}$ is a multilayer perceptron (MLP) with learnable parameters θ and output initialized close to zero (He et al., 2015). The softmax is applied over each row. Note that $\Delta = 0$ recovers the control histogram.

3.5 Training Objective

We train the model by minimizing a loss that compares the predicted (\hat{h}) and target (h) distributions using two components: (i) the Wasserstein-1 (W1) distance for distributional alignment and (ii) mean squared error (MSE) to match mean expressions. While cross-entropy is used for histogram prediction in other contexts (Imani et al., 2024), it treats bins independently and ignores the geometry of the support. In contrast, the W1 distance accounts for mass transport across bins and better reflects the continuity of expression data.

W1 term. For general 1D distributions, the W1 distance is given by $\text{W1} = \int_{-\infty}^{\infty} |\hat{F}(x) - F(x)| dx$, where \hat{F} and F are the predicted and true cumulative distribution functions (CDFs). For histogram distributions, we can compute this integral in closed form, as described below.

Let $I_{gb} = [x_{gb}^{(l)}, x_{gb}^{(r)}]$ be the b -th bin interval for gene g (with width w_g), to which the predicted and true histograms assign masses \hat{h}_{gb} and h_{gb} given a perturbation. The CDF gaps at the left and right bin edges are

$$C_{gb}^- = \hat{F}_g(x_{gb}^{(l)}) - F_g(x_{gb}^{(l)}) \quad \text{and} \quad C_{gb}^+ = \hat{F}_g(x_{gb}^{(r)}) - F_g(x_{gb}^{(r)}). \quad (3)$$

Assuming the densities are uniform inside I_{gb} , the gap varies linearly as follows (for $x \in I_{gb}$):

$$\hat{F}_g(x) - F_g(x) = C_{gb}^- + \frac{\delta_{gb}}{w_g}(x - x_{gb}^{(l)}), \quad (4)$$

where $\delta_{gb} = C_{gb}^+ - C_{gb}^- = \hat{h}_{gb} - h_{gb}$ represents the overall change. Integrating Eq. 4 over I_{gb} gives its exact contribution to the W1 distance:

$$\text{W1}_{gb} = \int_{I_{gb}} |\hat{F}_g(x) - F_g(x)| dx = \begin{cases} \frac{w_g}{2} (|C_{gb}^-| + |C_{gb}^+|) & \text{if } C_{gb}^- C_{gb}^+ \geq 0 \\ \frac{w_g}{2} \frac{|C_{gb}^-|^2 + |C_{gb}^+|^2}{|C_{gb}^-| + |C_{gb}^+|} & \text{if } C_{gb}^- C_{gb}^+ < 0. \end{cases} \quad (5)$$

The W1 loss is thus obtained by summing Eq. 5 over the B bins and averaging over all genes:

$$\mathcal{L}_{\text{wass}} = \frac{1}{G} \sum_{g=1}^G \sum_{b=1}^B \text{W1}_{gb}. \quad (6)$$

MSE term. This term resolves cases where several histograms share the same W1 distance from the control distribution and is defined as

$$\mathcal{L}_{\text{mse}} = \frac{1}{G} \sum_{g=1}^G (\hat{\mu}_g - \mu_g)^2, \quad \text{where} \quad \hat{\mu}_g = \sum_{b=1}^B \frac{1}{2} (x_{gb}^{(l)} + x_{gb}^{(r)}) \hat{h}_{gb} \quad (7)$$

is the predicted mean and μ_g is the target mean expression of gene g (for the given perturbation).

Total loss. We average the two components over perturbations and combine them with fixed weights:

$$\mathcal{L}_{\text{total}} = \lambda_{\text{wass}} \mathcal{L}_{\text{wass}} + \lambda_{\text{mse}} \mathcal{L}_{\text{mse}}, \quad (8)$$

where $\lambda_{\text{wass}} + \lambda_{\text{mse}} = 1$. The loss $\mathcal{L}_{\text{total}}$ is minimized over model parameters θ .

We provide Python code for our training procedure on GitHub⁵.

4 Experiments

4.1 Experimental Details

We evaluate our method on three single-cell Perturb-seq datasets across two cell lines. These include 102 single-gene perturbations in the K562 cell line from Norman et al. (2019), as well as 1076 (K562) and 1517 (RPE1) perturbations from Replogle et al. (2022). Gene expression values are log-normalized. We train and evaluate all models on single-gene perturbations. We employ 9-fold cross-validation to evaluate generalization to unseen perturbations, given the limited dataset size. Training is done on a single NVIDIA A40 GPU (45 GB) and takes 10-15 minutes per fold, depending on histogram resolution. We use 15 bins by default.

Histogram models are trained with a weighted sum of the W1 and MSE losses. A coarse grid sweep identified the best configuration as $\lambda_{\text{wass}} = 0.75$ and $\lambda_{\text{mse}} = 0.25$ (see Appendix C for details). We vary the MLP size with dataset scale to reduce overfitting: hidden dimensions are (1024, 512, 1024) for the Replogle data and (128, 64) for the smaller Norman dataset. Hidden layers use Layer Normalization (Ba et al., 2016) followed by a Leaky ReLU activation with negative slope 0.01. The output layer is linear. Models are trained using the AdamW optimizer (Loshchilov and Hutter, 2017) with learning rate 10^{-3} , weight decay 10^{-3} , dropout 0.2, and batch size 32, for 500 epochs per fold. Details of resource usage for training are provided in Appendix B.

4.2 Distributional Baselines & Evaluation

To assess how well our model captures post-perturbation gene expression distributions, we construct several baselines as described below.

First, *Ctrl Hist* predicts the control distribution h_{ctrl} for all perturbations. This represents a naive baseline that assumes no response to intervention. Second, *Non-Ctrl Hist* pools all perturbed cells in the training set and fits common per-gene histograms to the resulting data. This captures the aggregate expression distribution across perturbations – which may fare well on average likelihood metrics – but cannot model perturbation-specific effects.

Third, to create a perturbation-aware baseline, we train an MLP ($\mathbb{R}^d \rightarrow \mathbb{R}^{G \times 2}$) to predict the parameters of a truncated Gaussian (TG) for each gene conditioned on the perturbation. This can capture coarse changes in the mean and variance, with truncation enforcing non-negative expressions and enabling fair comparison with the bounded supports used by the histogram model (Eq. 1). The TG density has the following general form on its support $[a, b]$:

$$f_{\text{TG}}(x; \mu, \sigma) = \frac{\frac{1}{\sigma\sqrt{2\pi}} e^{-\frac{1}{2}\left(\frac{x-\mu}{\sigma}\right)^2}}{\Phi\left(\frac{b-\mu}{\sigma}\right) - \Phi\left(\frac{a-\mu}{\sigma}\right)}, \quad \text{where} \quad \Phi(x) = \frac{1}{2} \left(1 + \text{erf}(x/\sqrt{2})\right) \quad (9)$$

⁵<https://github.com/Kalyan0821/LLMHistPert>

and parameters (μ, σ) describe the underlying Gaussian truncated to $[a, b]$. In our case, given perturbation p , the model outputs G pairs $(\mu_{g,\theta}(p), \log \sigma_{g,\theta}(p))$ corresponding to supports $r_g = [a_g, b_g]$. We also constrain $\mu_{g,\theta}$ to $[a_g - 1.5\sigma_U, b_g + 1.5\sigma_U]$, where $\sigma_U = (b_g - a_g)/\sqrt{12}$ is the standard deviation of a uniform distribution over r_g . This prevents the model from pushing $\mu_{g,\theta}$ far outside the observed data range, which may cause vanishing likelihoods and unstable training.

Finally, to account for the prevalence of zero-valued observations in single-cell data, we define a zero-inflated truncated Gaussian (*ZITG*) density with the following general form:

$$f_{\text{ZITG}}(x; \mu, \sigma, \pi) = \pi \mathcal{U}_{[-\epsilon, \epsilon]}(x) + (1 - \pi) f_{\text{TG}}(x; \mu, \sigma), \quad (10)$$

where the extra parameter $\pi \in [0, 1]$ represents the zero-inflation probability and $\mathcal{U}_{[-\epsilon, \epsilon]}$ is a narrow uniform density of width 2ϵ centred at the origin. In our case, given perturbation p , the MLP ($\mathbb{R}^d \rightarrow \mathbb{R}^{G \times 2} \times [0, 1]^G$) produces G triplets $(\mu_{g,\theta}(p), \log \sigma_{g,\theta}(p), \pi_{g,\theta}(p))$ corresponding to the supports r_g and half-widths ϵ_g defined in Eq. 1.

Baseline training. For the TG and ZITG baselines, we minimize the average negative log-likelihood (NLL) of the training data. Given a perturbation, the NLL of gene g 's expressions is

$$\text{NLL}_g = -\frac{1}{N_g} \sum_{n=1}^{N_g} \log f(x_{gn}; \theta), \quad (11)$$

where N_g is the number of post-perturbation samples of gene g . The average NLL is then obtained by averaging this over all genes and perturbations in the dataset.

Evaluating distributions. For each method, we report the average NLL over unseen perturbations to test if the predicted distributions fit the observed expression values. Note that for the histogram model, NLLs can be obtained efficiently without evaluating on the samples $\{x_{gn}\}$ each time as follows:

$$\text{NLL}_g^{\text{hist}} = -\sum_{b=1}^B h_{gb} \log \left(\frac{\hat{h}_{gb}}{w_g} \right). \quad (12)$$

We also test the ability to represent perturbation-specific structure by reporting errors in *statistics* of the predicted distributions compared to the observed data. Specifically, we compute the relative mean absolute errors (RMAE) of the predicted mean, variance, skewness, and excess kurtosis. Statistics are obtained from the parameters of the TG / ZITG and the bin probabilities of the histogram model (see Appendix A for details). Given an unseen perturbation, the RMAE of statistic τ is given by

$$\text{RMAE}(\hat{\tau}, \tau) = \frac{\sum_{g=1}^G |\hat{\tau}_g - \tau_g|}{\sum_{g=1}^G |\tau_g|}, \quad (13)$$

where $\hat{\tau}_g$ and τ_g denote its predicted and observed value for gene g . We average this error over all perturbations in the test set, serving as a ‘‘shape-aware’’ distributional metric.

4.3 Quantitative Results

Table 1 compares our histogram model (*MLP+Hist*) to the distributional baselines on unseen perturbations from the two Replogle cell lines. On both, *MLP+Hist* achieves the lowest RMAE for all four statistics, with the improvement over *ZITG* increasing with the moment order (e.g., from 1.8% in the mean to 10.2% in kurtosis, on K562). This behavior is learned entirely from the expression data, unlike *TG / ZITG* that fix the functional form of the distribution, enabling greater flexibility to represent perturbation-specific structure. As expected, *ZITG* outperforms *TG* on all metrics, given the extra flexibility from the zero-inflation component.

Moreover, Table 1 shows that *MLP+Hist* offers **significantly higher data efficiency**, training $\sim 2.5\times$ faster than *ZITG* on K562 and $3.3\times$ faster on RPE1. We also analyze the memory usage of the methods in Appendix B, where *MLP+Hist* has only a fraction of the requirements of *TG / ZITG*. This is because rather than optimizing for hundreds of post-perturbation samples per gene, *MLP+Hist* trains on a fixed-size, compressed version of this data (15 bin heights per gene). Still, our method generalizes more effectively to unseen perturbations, demonstrating that learning histogram representations is a straightforward and scalable approach to modeling genetic perturbation effects.

Cell line	Method	NLL (\downarrow)	Mean	RMAE (\downarrow)			Train time (\downarrow) (mins/fold)
				Var	Skew	Kurt	
K562	Ctrl Hist	-0.379	1.000	0.184	0.237	0.572	N/A
	Non-Ctrl Hist	-0.393	0.980	0.213	0.235	0.590	N/A
	TG (LLM)	0.016	0.934	0.250	0.472	0.940	20.49
	ZITG (LLM)	-0.381	0.895	0.182	0.241	0.600	24.52
	MLP+Hist (LLM)	-0.388	0.879	0.175	0.225	0.539	9.89
RPE1	Ctrl Hist	-0.437	1.000	0.269	0.308	0.685	N/A
	Non-Ctrl Hist	-0.459	0.895	0.266	0.284	0.665	N/A
	TG (LLM)	-0.068	0.896	0.302	0.461	0.899	41.16
	ZITG (LLM)	-0.455	0.865	0.242	0.281	0.655	49.49
	MLP+Hist (LLM)	-0.441	0.863	0.239	0.276	0.633	14.93

Table 1: Distributional model performance on unseen perturbations from the two Replogle cell lines. For each method, we report the gene-averaged NLL and RMAEs of post-perturbation statistics.

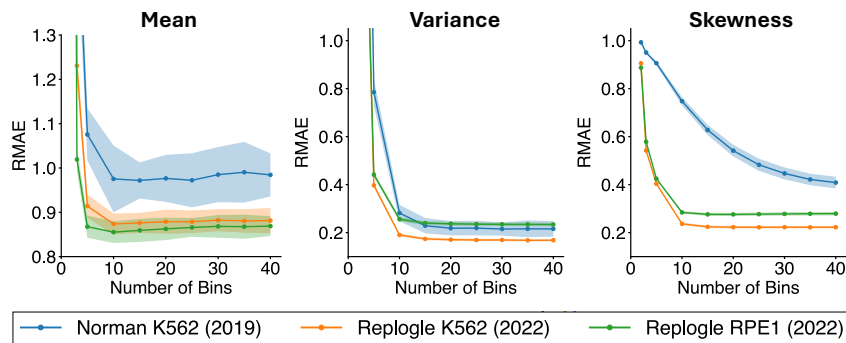


Figure 2: Effect of histogram resolution on the prediction error of post-perturbation statistics for three benchmark datasets. Performance improves with resolution but plateaus at 15-20 bins on the larger Replogle datasets. Shading indicates the standard deviation across folds.

Interestingly, *Non-Ctrl Hist* attains the best NLL on both cell lines. This can be attributed to the pooled (global) histogram assigning a substantial mass to the zero-expression bin ($\sim 61\%$ in K562 and 64% in RPE1), which accounts for the majority of single-cell measurement data. However, since it predicts the same histogram for every perturbation, it cannot represent perturbation-specific shifts and performs significantly worse on the shape-aware metrics (Table 1).

Effect of Histogram Resolution. Fig. 2 shows how model performance varies with histogram resolution. On the Replogle data, as the number of bins increases, the RMAEs of the mean, variance, and skewness steadily improve before plateauing at 15–20 bins, suggesting that a moderate resolution is sufficient to recover statistical features while maintaining computational efficiency. The improvement is less consistent across statistics on the Norman dataset, likely due to its relatively small training set size of around 90 perturbations per fold, compared to 1000 in Replogle.

4.4 Qualitative Results

To qualitatively assess the predicted distributional shifts, we plot W1 distances between the control and predicted distributions $W1(\hat{h}_g, h_g^{\text{ctrl}})$ vs. those between the control and observed distributions $W1(h_g, h_g^{\text{ctrl}})$ for all genes g given an unseen perturbation. Fig. 3 (left) shows this plot for two example perturbations (CDKN1B⁶ and POU3F2⁷), where each circle represents a gene. The plot provides a global view of distributional shift accuracy, helping identify genes where predictions

⁶<https://www.ncbi.nlm.nih.gov/gene/1027>

⁷<https://www.ncbi.nlm.nih.gov/gene/5454>

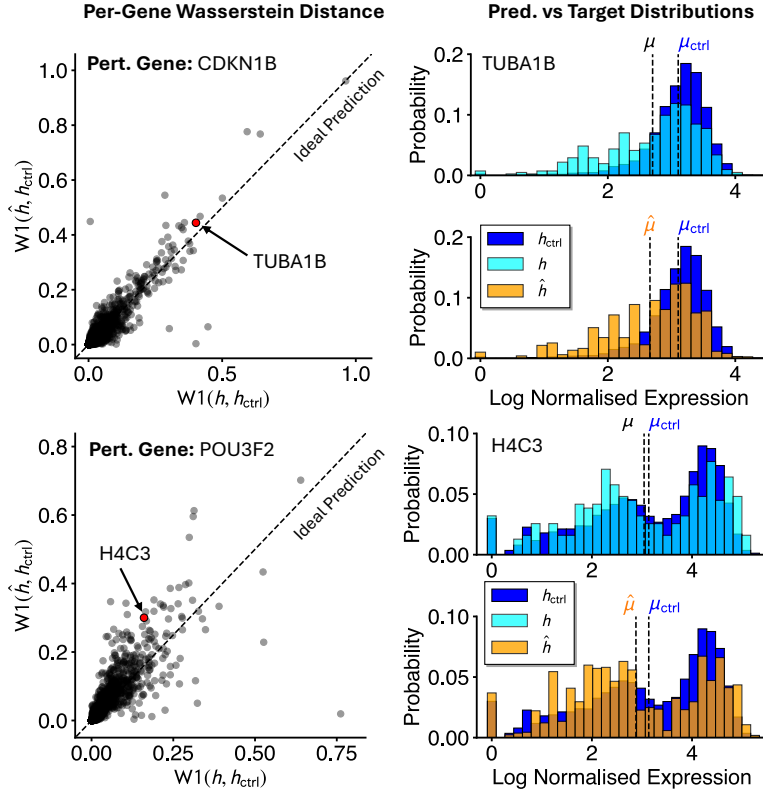


Figure 3: Distributional shift plots (left) and highlighted gene expression histograms (right) (using 35 bins) following two example perturbations (CDKN1B and POU3F2) from the Norman data. Each circle represents a gene g with coordinates $x = W1(h_g, h_g^{ctrl})$ and $y = W1(\hat{h}_g, h_g^{ctrl})$, measuring the observed and predicted shifts from the control distribution (dark blue), respectively. We include histograms for two genes that exhibit non-mean effects: (i) TUBA1B, which shows increased variance, and (ii) H4C3, which has a multimodal response. In both cases, predicted histograms (orange) closely match the post-perturbation data (cyan). Vertical dashed lines mark the means.

succeed or fail (ideal predictions lie along the diagonal). We examine two genes (TUBA1B⁸ and H4C3⁹) exhibiting distinct non-mean effects that our model recovers effectively.

TUBA1B encodes a tubulin alpha chain involved in building the cell’s internal structure and regulating cell-cycle progression (Wang et al., 2024). Its expression in control cells is tightly clustered. CDKN1B (perturbed gene) restrains cell division by putting a checkpoint on the DNA replication phase – when this gene is knocked down, the checkpoint is lost, causing cells to progress through the cycle asynchronously (Sun et al., 2016). As a result, the TUBA1B expression becomes more variable across the population. As seen in Fig. 3 (top right), *MLP+Hist* captures this increase in variance (and reduction in mean), demonstrating the ability to predict higher-order effects beyond the mean.

H4C3, a histone gene involved in DNA packaging and gene regulation (Seal et al., 2022), shows a bimodal distribution in control conditions, indicating distinct transcriptional states. When POU3F2 is knocked down, more cells enter the low-expression state, and fewer remain high (Eisen et al., 1995). As seen in Fig. 3 (bottom right), *MLP+Hist* captures this change in proportions (although the mean hardly changes and peak positions remain stable), highlighting the ability to predict subtle yet biologically relevant shifts.

⁸<https://www.ncbi.nlm.nih.gov/gene/10376>

⁹<https://www.ncbi.nlm.nih.gov/gene/8364>

Cell line	Method	Pearson correlation (\uparrow)			RMAE (\downarrow)
		Top 20	Top 50	Top 100	
K562	Non-Ctrl Mean	0.460 \pm 0.03	0.495 \pm 0.02	0.513 \pm 0.02	0.981 \pm 0.01
	GEARS	0.472 \pm 0.03	0.504 \pm 0.03	0.513 \pm 0.03	1.050 \pm 0.02
	GP (LLM)	0.656 \pm 0.03	0.702 \pm 0.03	0.706 \pm 0.02	0.869 \pm 0.02
	MLP+Mean (LLM)	0.658 \pm 0.02	0.701 \pm 0.02	0.710 \pm 0.02	0.871 \pm 0.03
	MLP+Hist (LLM)	0.653 \pm 0.03	0.697 \pm 0.02	0.703 \pm 0.02	0.876 \pm 0.02
RPE1	Non-Ctrl Mean	0.654 \pm 0.03	0.702 \pm 0.02	0.723 \pm 0.02	0.893 \pm 0.03
	GEARS	0.553 \pm 0.02	0.621 \pm 0.03	0.660 \pm 0.03	0.955 \pm 0.03
	MLP+Mean (LLM)	0.685 \pm 0.03	0.733 \pm 0.02	0.756 \pm 0.02	0.860 \pm 0.03
	MLP+Hist (LLM)	0.672 \pm 0.03	0.726 \pm 0.02	0.749 \pm 0.02	0.859 \pm 0.02

Table 2: Mean prediction performance (\pm standard deviation across folds) on unseen perturbations from the two Replogle cell lines. For each method, we report correlations (between predicted and observed mean shifts) over the top differentially expressed (DE) genes and RMAE over all genes.

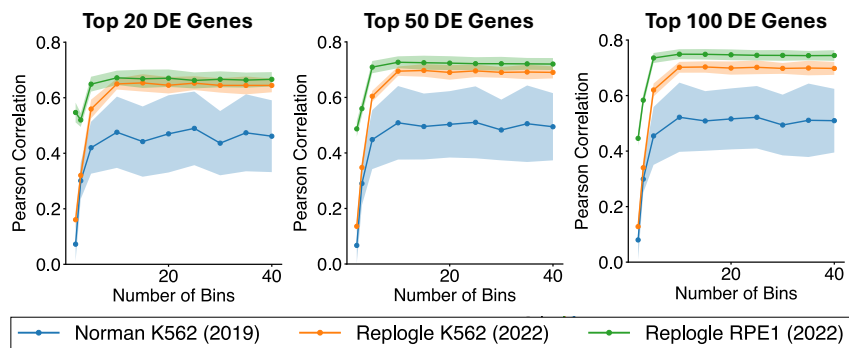


Figure 4: Effect of histogram resolution on the correlation between predicted and true mean shifts over the top differentially expressed (DE) genes for three benchmark datasets. Performance improves with resolution but plateaus at 15-20 bins. Shading indicates the standard deviation across folds.

Detecting variance inflation in a cell-cycle gene or shifts in chromatin states provides mechanistic insights inaccessible to point-estimate methods. Thus, the histogram model has the potential to offer a more informative basis for biological hypothesis generation than models limited to mean expression.

4.5 Comparison to Mean-based Methods

We evaluate mean prediction performance separately to compare *MLP+Hist* with existing methods that predict only mean expression shifts (as a sanity check). Of these, we consider the graph-based *GEARS* (Roohani et al., 2024) and the recent LLM-based Gaussian process regressor (*GP*) by Märtens et al. (2024). We also consider two baselines: (i) *Non-Ctrl Mean*, which predicts the per-gene mean expression over all perturbed cells in the training set – incorporating global response trends but not perturbation identity, and (ii) *MLP+Mean*, where we train an MLP ($\mathbb{R}^d \rightarrow \mathbb{R}^G$) with the same architecture as *MLP+Hist* to predict per-gene shifts in mean expression – representing a perturbation-aware baseline. We exclude methods like scGPT (Cui et al., 2024) since it was shown to be easily outperformed by *GEARS* / *Non-Ctrl Mean* (Ahlmann-Eltze et al., 2024; Märtens et al., 2025).

Following prior work (Bereket and Karaletsos, 2023; Roohani et al., 2024), for each method, we report the perturbation-averaged (i) Pearson correlation between predicted ($\hat{\mu} - \mu_{\text{ctrl}}$) and observed ($\mu - \mu_{\text{ctrl}}$) mean shifts – calculated separately over the top 20, 50, and 100 differentially expressed (DE) genes, and (ii) RMAE of the predicted mean shift. Focusing on differences relative to control penalizes models that replicate the mean control expression, which can have a deceptively high correlation with the observed mean (Märtens et al., 2024).

Table 2 compares the mean-based methods on unseen perturbations from the two Replogle cell lines. On both, *MLP+Hist* performs similarly to the other LLM-based models, including the dedicated mean regressor *MLP+Mean*, while modeling a richer output space. It also outperforms *Non-Ctrl Mean* and earlier approaches like GEARS on all metrics. Interestingly, the simple *Non-Ctrl Mean* baseline significantly outperforms GEARS on RPE1 and gets close on K562, further highlighting the advantage of LLM-derived biological priors for generalizable perturbation response prediction.

Effect of Histogram Resolution. Fig. 4 shows how *MLP+Hist* performance varies with histogram resolution. Correlations improve with increasing bin count and plateau at 15-20 bins, confirming that a moderate resolution is sufficient to recover shifts in mean expression as well.

5 Conclusion

We introduced a neural network that predicts gene expression distributional shifts using LLM embeddings of unseen genetic perturbations with a histogram-based output. Through experiments on standard Perturb-seq datasets, we showed that this simple method (i) outperforms baselines in predicting distributional structure at a much lower training cost, (ii) can reveal mechanistic insights that may enable improved hypothesis generation in genomics, and (iii) is competitive with other methods in predicting mean expression changes. It also highlights the benefit of LLM-based biological priors for generalization to unseen perturbations.

We end with some limitations and suggestions for future work. First, predictions are constrained by the expression range observed during training due to the histogram representation, which limits extrapolation and requires truncated baselines for fair comparison. Second, the method treats genes independently by modeling marginal distributions but not the regulatory dependencies between genes. Future work could explore methods for efficiently modeling this high-dimensional joint distribution. Third, while we use a simple discrete representation, continuous alternatives, such as kernel density estimation (KDE), could improve flexibility and extrapolation, albeit with higher modeling complexity. Finally, future work should focus more on extracting valuable biological insights from distributional models to assess the practical utility of our approach better.

Acknowledgements

KR is supported by the EPSRC Centre for Doctoral Training in Autonomous Intelligent Machines and Systems EP/S024050/1. JGH is supported by a Novo Nordisk Postdoctoral Fellowship in partnership with the University of Oxford. SQ is supported by Wellcome Trust in partnership with the University of Oxford.

References

- C. Ahlmann-Eltze, W. Huber, and S. Anders. Deep learning-based predictions of gene perturbations effects do not yet outperform simple linear baselines. *bioRxiv*, 2024.09.16.613342, 2024.
- J. L. Ba, J. R. Kiros, and G. E. Hinton. Layer Normalization. *arXiv preprint arXiv:1607.06450*, 2016.
- M. Bereket and T. Karaletsos. Modelling cellular perturbations with the sparse additive mechanism shift variational autoencoder. *NeurIPS*, 2023.
- C. Bunne, S. G. Start, and G. G. et al. Learning single-cell perturbation responses using neural optimal transport. *Nature Methods*, 20:1759–1768, 2023.
- Y. Chen and J. Zou. GenePT: A simple but effective foundation model for genes and cells built from ChatGPT. *bioRxiv*, 2023.10.16.562533, 2024.
- H. Cui, C. Wang, H. Maan, K. Pang, F. Luo, N. Duan, and B. Wang. scGPT: toward building a foundation model for single-cell multi-omics using generative AI. *Nature Methods*, 21:1470–1480, 2024.
- L. de Torrenté, S. Zimmerman, M. Suzuki, M. Christopheit, J. M. Greally, and J. C. Mar. The shape of gene expression distributions matter: how incorporating distribution shape improves the interpretation of cancer transcriptomic data. *BMC Bioinformatics*, 21:562, 2020.

- A. Dixit, O. Parnas, B. Li, J. Chen, C. P. Fulco, L. Jerby-Arnon, N. D. Marjanovic, D. Dionne, T. Burks, R. Raychowdhury, B. Adamson, T. M. Norman, E. S. Lander, J. S. Weissman, N. Friedman, and A. Regev. Perturb-Seq: Dissecting Molecular Circuits with Scalable Single-Cell RNA Profiling of Pooled Genetic Screens. *Cell*, 167:1853–1866, 2016.
- T. Eisen, D. J. Easty, D. C. Bennett, and C. R. Goding. The POU domain transcription factor Brn-2: elevated expression in malignant melanoma and regulation of melanocyte-specific gene expression. *Oncogene*, 11(10):2157–2164, 1995.
- A. Elnaggar, M. Heinzinger, C. Dallago, G. Rehawi, Y. Wang, L. Jones, T. Gibbs, T. Feher, C. Angerer, M. Steinegger, D. Bhowmik, and B. Rost. ProtTrans: Toward Understanding the Language of Life Through Self-Supervised Learning. *IEEE Transactions on Pattern Analysis and Machine Intelligence*, 44:7112–7127, 2022.
- M. Hao, J. Gong, X. Zeng, C. Liu, Y. Guo, X. Cheng, T. Wang, J. Ma, X. Zhang, and L. Song. Large-scale foundation model on single-cell transcriptomics. *Nature Methods*, 2024.
- K. He, X. Zhang, S. Ren, and J. Sun. Delving deep into rectifiers: Surpassing human-level performance on imagenet classification. In *Proceedings of the IEEE international conference on computer vision*, pages 1026–1034, 2015.
- E. Imani, K. Luedemann, S. Scholnick-Hughes, E. Elelimy, and M. White. Investigating the Histogram Loss in Regression. *arXiv*, 2402.13425, 2024.
- D. P. Kingma, M. Welling, et al. Auto-Encoding Variational Bayes, 2013.
- R. Lopez, J. Regier, M. B. Cole, M. I. Jordan, and N. Yosef. Deep generative modeling for single-cell transcriptomics. *Nature Methods*, 15:1053–1058, 2018.
- R. Lopez, N. Tagasovska, S. Ra, K. Cho, J. Pritchard, and A. Regev. Learning Causal Representations of Single Cells via Sparse Mechanism Shift Modeling. In *Proceedings of the Second Conference on Causal Learning and Reasoning*, volume 213 of *Proceedings of Machine Learning Research*, pages 662–691, 2023.
- I. Loshchilov and F. Hutter. Decoupled Weight Decay Regularization. *arXiv preprint arXiv:1711.05101*, 2017.
- M. Lotfollahi, F. A. Wolf, and F. J. Theis. scGen predicts single-cell perturbation responses. *Nature Methods*, 16:715–721, 2019.
- M. Lotfollahi, A. K. Susmelj, and C. D. D. et al. Predicting cellular responses to complex perturbations in high-throughput screens. *Molecular Systems Biology*, 19:e11517, 2023.
- K. Märtens, R. Donovan-Maiye, and J. Ferkinghoff-Borg. Enhancing generative perturbation models with LLM-informed gene embeddings. In *ICLR 2024 Workshop on Machine Learning for Genomics Explorations*, 2024.
- K. Märtens, M. B. Martell, C. A. Prada-Medina, and R. Donovan-Maiye. LangPert: LLM-Driven Contextual Synthesis for Unseen Perturbation Prediction. In *ICLR 2025 Workshop on Machine Learning for Genomics Explorations*, 2025.
- T. M. Norman, M. A. Horlbeck, J. M. Replogle, A. Y. Ge, A. Xu, M. Jost, L. A. Gilbert, and J. S. Weissman. Exploring genetic interaction manifolds constructed from rich single-cell phenotypes. *Science*, 365:786–793, 2019.
- J. Paulsson. Models of stochastic gene expression. *Physics of Life Reviews*, 2:157–175, 2005.
- A. Raj and A. van Oudenaarden. Nature, Nurture, or Chance: Stochastic Gene Expression and its Consequences. *Cell*, 135:216–226, 2008.
- J. M. Replogle, R. A. Saunders, and A. N. P. et al. Mapping information-rich genotype-phenotype landscapes with genome-scale perturb-seq. *Cell*, 185:2559–2575, 2022.

- A. Rives, J. Meier, T. Sercu, and R. Fergus. Biological structure and function emerge from scaling unsupervised learning to 250 million protein sequences. *Proc. Natl. Acad. Sci. U.S.A.*, 118: e2016239118, 2021.
- Y. Roohani, K. Huang, and J. Leskovec. Predicting transcriptional outcomes of novel multigene perturbations with GEARS. *Nature Biotechnology*, 42:927–935, 2024.
- R. L. Seal, P. Denny, E. A. Bruford, A. K. Gribkova, D. Landsman, W. F. Marzluff, M. McAndrews, A. R. Panchenko, A. K. Shaytan, and P. B. Talbert. A standardized nomenclature for mammalian histone genes. *Epigenetics & Chromatin*, 15:34, 2022.
- C. Sun, G. Wang, K. H. Wrighton, H. Lin, Z. Songyang, X.-H. Feng, and X. Lin. Regulation of p27Kip1 phosphorylation and G1 cell cycle progression by protein phosphatase PPM1G. *American Journal of Cancer Research*, 6(10):2207–2220, 2016.
- C. V. Theodoris, L. Xiao, A. Chopra, M. D. Chaffin, Z. R. A. Sayed, M. C. Hill, H. Mantineo, E. M. Brydon, Z. Zeng, X. S. Liu, and P. T. Ellinor. Transfer learning enables predictions in network biology. *Nature*, 618:616–624, 2023.
- Y. Wang, Y. Li, Y. Jing, Y. Yang, H. Wang, D. Ismtula, and C. Guo. TUBA1B promotes proliferation and migration in hepatocellular carcinoma. *Scientific Reports*, 14:8201, 2024.
- Y. Wu, E. Wershof, S. M. Schmon, M. Nassar, B. Osiński, R. Eksi, K. Zhang, and T. Graepel. PerturBench: Benchmarking Machine Learning Models for Cellular Perturbation Analysis. In *NeurIPS 2024 Workshop on AI for New Drug Modalities*, 2024.

Appendix

A Higher-order Statistics

We calculate the variance, skewness, and excess kurtosis of a distribution from its raw moments $m_k = \mathbb{E}[X^k]$, where $k \in \{1, 2, 3, 4\}$, using the following formulas:

$$\begin{aligned}\text{Var}[X] &= m_2 - m_1^2 \\ \text{Skew}[X] &= \frac{m_3 - 3 m_1 m_2 + 2 m_1^3}{\text{Var}[X]^{3/2}} \\ \text{Kurt}[X] &= \frac{m_4 - 4 m_1 m_3 + 6 m_1^2 m_2 - 3 m_1^4}{\text{Var}[X]^2} - 3.\end{aligned}$$

We specify the moment expressions for each distribution below.

Histogram. Given a histogram with B bin intervals $[x_b^{(l)}, x_b^{(r)}]$ of widths w_b having probabilities h_b ,

$$m_k^{\text{hist}} = \sum_{b=1}^B \frac{(x_b^{(r)})^{k+1} - (x_b^{(l)})^{k+1}}{k+1} \frac{h_b}{w_b}.$$

TG. Given parameters (μ, σ) and support $[a, b]$,

$$m_k^{\text{TG}} = \sum_{r=0}^k \binom{k}{r} \mu^{k-r} \sigma^r L_r,$$

with

$$\begin{aligned}L_0 &= 1 \\ L_1 &= -\frac{\varphi(\beta) - \varphi(\alpha)}{\Phi(\beta) - \Phi(\alpha)} \\ L_r &= -\frac{\beta^{r-1}\varphi(\beta) - \alpha^{r-1}\varphi(\alpha)}{\Phi(\beta) - \Phi(\alpha)} + (r-1)L_{r-2}, \quad r \geq 2,\end{aligned}$$

where $\alpha = (a - \mu)/\sigma$, $\beta = (b - \mu)/\sigma$, and $\varphi(\cdot)$ and $\Phi(\cdot)$ are the density and CDF of the standard normal distribution¹⁰.

ZITG. Given zero-inflation probability π , TG parameters (μ, σ) , and support $[a, b]$,

$$m_k^{\text{ZITG}} = \pi m_k^{\mathcal{U}} + (1 - \pi) m_k^{\text{TG}},$$

where the moments of the uniform spike $\mathcal{U}_{[-\epsilon, \epsilon]}$ are given by

$$m_k^{\mathcal{U}} = \frac{1 - (-1)^{k+1} \frac{\epsilon^k}{2}}{k+1}.$$

B Resource Use for Training

Table 3 compares the training time, peak GPU memory usage, and learnable parameters of several methods described in this work for the two Replogle cell lines. Among the learnable distributional models, *MLP+Hist* is both the quickest to train and the lightest in terms of memory usage despite carrying more parameters. For example, on the RPE1 data, it trains ~ 2.7 - $3.3x$ faster than the *TG* / *ZITG* baselines and requires $\sim 8.2x$ less memory to train.

The extra cost for the distributional baselines is due to the need to calculate and optimize log-likelihoods for every post-perturbation sample per gene. Moreover, since the number of cells varies across perturbations, the data is padded up to the largest sample size in its mini-batch, wasting computation and increasing memory usage. In contrast, *MLP+Hist* learns from a fixed-size compression of the data, enabling simple and scalable modeling of genetic perturbation effects.

¹⁰https://people.sc.fsu.edu/~jburkardt/presentations/truncated_normal.pdf

Cell line	Method	Train time (mins per fold)	GPU Memory Usage (MB)	Learnable Params
K562	Non-Ctrl Mean	N/A	1,013	N/A
	Non-Ctrl Hist	N/A	1,617	N/A
	MLP+Mean (LLM)	3.14	1,575	8,802,696
	MLP+Hist (LLM)	9.89	3,219	80,552,696
	TG (LLM)	20.49	10,735	13,927,696
	ZITG (LLM)	24.52	12,023	19,052,696
RPE1	Non-Ctrl Mean	N/A	1,091	N/A
	Non-Ctrl Hist	N/A	1,885	N/A
	MLP+Mean (LLM)	4.47	1,655	8,802,696
	MLP+Hist (LLM)	14.93	3,503	80,552,696
	TG (LLM)	41.16	28,970	13,927,696
	ZITG (LLM)	49.49	28,710	19,052,696

Table 3: Training costs of methods when trained on a single NVIDIA A40 GPU.

C Hyperparameters

We experiment with using a weighted sum of three loss terms,

$$\mathcal{L}_{\text{total}} = \lambda_{\text{ce}}\mathcal{L}_{\text{ce}} + \lambda_{\text{wass}}\mathcal{L}_{\text{wass}} + \lambda_{\text{mse}}\mathcal{L}_{\text{mse}},$$

where $\lambda_{\text{ce}} + \lambda_{\text{wass}} + \lambda_{\text{mse}} = 1$ and \mathcal{L}_{ce} is a simple cross-entropy loss (which we average over perturbations in the training set):

$$\mathcal{L}_{\text{ce}} = -\frac{1}{G} \sum_{g=1}^G \sum_{b=1}^B h_{gb} \log \hat{h}_{gb}.$$

We perform a coarse grid search (with step size 0.25) over valid triples $(\lambda_{\text{ce}}, \lambda_{\text{wass}}, \lambda_{\text{mse}})$ and report mean-shift prediction performance for the Replogle K562 cell line in Table 4. The best configuration ($\lambda_{\text{wass}} = 0.75$ and $\lambda_{\text{mse}} = 0.25$) assigns a majority weight to the Wasserstein term and retains the MSE contribution. Adding even a small weight to the cross-entropy loss hurts performance, with the worst configuration assigning all of the weight to it.

λ_{ce}	λ_{wass}	λ_{mse}	Corr. Top 20 (\uparrow)
1	0	0	0.628
0.5	0	0.5	0.635
0.25	0	0.75	0.636
0.75	0	0.25	0.638
0.75	0.25	0	0.639
0.25	0.5	0.25	0.639
0.25	0.75	0	0.644
0.25	0.25	0.5	0.644
0.5	0.5	0	0.647
0	1	0	0.647
0	0.25	0.75	0.647
0	0.5	0.5	0.648
0	0.75	0.25	0.651

Table 4: Effect of the loss weights used to train the histogram model.